DANISH METEOROLOGICAL INSTITUTE

TECHNICAL REPORT

99-14

Evaluation of Skin-Bulk Sea Surface Temperature Difference Models for use in the Ocean and Sea Ice SAF

July 1999

Brett Candy (UKMO)
Søren Andersen (DMI)

ISSN 0906-897X (printed form)
ISSN 1399-1388 (online form)

Copenhagen 1999

List of contents

1. Introduction

The work of the Ocean and Sea Ice SAF (Satellite Application Facility) has included the development of SST retrieval algorithms for infra-red radiometers on both polar-orbiting and geostationary platforms. These algorithms have been derived (by regressing surface temperatures against simulated radiances) so that they attempt to retrieve the surface *skin* SST (Andersen et al, 1998). For meteorological studies this is perhaps the desired quantity since it represents the interface temperature between the atmosphere and ocean. However for many other applications, such as climate research and oceanography, what is required is the temperature of the mixed layer or the *bulk* SST. Since infra-red radiation cannot penetrate to this depth a method of conversion from skin SST to bulk SST is required which can easily be applied to satellite observations. One method to do this is to simply bias correct the satellite observations with respect to co-located in-situ bulk SST measurements. A more attractive approach is to model the temperature difference across the skin layer.

Various researchers have proposed skin layer models, with the skin represented as a conduction layer. Below this layer the ocean is considered to be well mixed at night (during the day a temperature gradient can build up in the mixed layer known as the diurnal thermocline). Depending on the direction of the heat flux between the ocean and atmosphere the skin SST can either be cooler or warmer than the underlying bulk SST value in a range of around ±1K. Table 1.1 lists the key properties of a selection of skin layer models. Each model requires an estimate of the surface windspeed or windstress and the net heat flux out of the ocean. Normally the solar contribution is ignored since the amount absorbed in the skin layer is small.

Model	**Type**	**windspeed regime**
Saunders (1967)	fixed conduction layer - depth dependant on windspeed	moderate to high
Fairall (1996)	extension of Saunders to low windspeed	low to high
Soloviev - Schlüssel (1994)	surface renewal	low to high

Table 1.1 *Properties of skin layer models.*

Several experiments at sea have tested these skin layer models using ship-borne radiometers to measure the skin SST and in-situ meteorological data to compute the surface fluxes. Kent et al (1996) found that the observed bulk-skin SST difference in a region south of the Azores could be best accounted for by the Saunders model. The model was also applicable during the day except under conditions of low windspeed when free convection prevails and high-insolation when a near surface thermocline developed.

In the case of satellite data, Candy & Harris (1998) tested a selection of skin models in order to produce bulk SSTs from the Along Track Scanning Radiometer (ATSR). They used fluxes and windspeeds from a Numerical Weather Prediction (NWP) model to drive the models and found that if low windspeed cases were neglected both the bias and standard deviation of the observed bulk-satellite SST difference could be reduced. The Saunders model gave the best performance and the observed global bulk-skin SST difference was found to be about 0.3K.

The authors have recently extended the work to cover the low windspeed regime using the Fairall model which is a development of the Saunders model to cover low windspeed conditions.

Skin layer models then have been shown to be useful for skin SST measurements made from spaceborne and shipborne radiometers. This report outlines an investigation into the use of such models to convert skin SST from the SAF algorithms to a bulk measurement. It is intended that operationally the SAF Atlantic product will use a combination of observations from geostationary instruments and from the Advanced Very High Resolution Radiometer (AVHRR). The work here concentrates on AVHRR data since the observations are global and have a lower noise level.

2. Models and measurements of the skin effect

The skin effect occurs due to the energy exchange between the ocean and the atmosphere. The skin layer is generally around 0.5 mm thick depending on the wind mixing and the heat transfer across it takes place by molecular conduction. The net flux through the skin is composed of four fluxes: latent, sensible, infrared and solar (short-wave). Due to the very small thickness of the skin layer only a small attenuation of the short-wave radiation takes place across it and the last term of the flux budget is therefore often omitted in considerations involving the skin layer (e.g. Kent et al., 1996). Depending on the direction of the heat flux the skin may be either warmer or colder than the mixed layer underneath. However, the heat flux across the skin layer is on average out of the ocean resulting in a skin that is cooler than the mixed layer. Increased mixing in the form of wind will tend to erode the skin layer and thereby lower the skin temperature difference. Based on previous results (e.g. Wick et al., 1996; Kent et al., 1996; Candy & Harris, 1998) two well performing algorithms, representing the fixed conduction layer and the surface renewal approach, will be considered.

Based on the requirement of continuity of the heat fluxes across the skin layer, Saunders (1967) derived the following formulation of the temperature difference across the skin:

$$\Delta T = \frac{\lambda Q \nu}{\kappa \rho c_p v_*} \tag{2.1}$$

where κ is the thermal diffusivity, ρ is the density of water, c_p is the specific heat capacity of water, v_* is the friction velocity in water, ν is the kinematic viscosity, Q the net heat flux and λ is a dimensionless constant. This formulation is applicable for forced convection, i.e. when the wind is sufficiently strong, typically more than 3 m/s. The value of λ was suggested by Saunders to be between 5 and 10 but was found to be between 2 and 5.5 increasing with windspeed by Grassl (1976). By blending the expression of Saunders for the thickness of the skin layer during forced convection with an expression for the skin layer thickness during free convection Fairall et al. (1996a) extended the Saunders formulation to also cover the free convection, i.e. low wind speed regime by defining:

$$\lambda = \lambda_0 \left(1 + \left(\frac{A^3 \lambda_0^4 Q g \alpha \rho c_p \nu^3}{v_*^4 \kappa^2} \right)^{3/4} \right)^{-1/3} \tag{2.2}$$

where g is gravity, α is the thermal expansion coefficient of sea water, A the convective coefficient suggested to be 0.23 and λ_0 is the value to which λ will tend with increasing wind speed when the Fairall model becomes equivalent to Saunders.

These formulations represent the fixed conduction layer models. Assuming the skin layer to be constantly renewed with water from the mixed layer below, the renewal timescale depending on the rate of turbulence and fluxes, a class of models termed surface renewal models have been developed by several authors. One of the more recent and general models

of this class is the one by Soloviev and Schlüssel (1994) describing the skin temperature difference as follows:

$$\Delta T = \Lambda_0 \, \mathrm{Pr}^{1/2} \frac{Q}{\rho c_p v_*} \left(1 + \frac{R_f}{R_{f_{cr}}}\right)^{-1/4} \left(1 + \frac{Ke}{Ke_{cr}}\right)^{1/2} \qquad (2.3)$$

where Pr is the Prandtl number, R_f is the Richardson number, Ke is the Keulegan number, $R_{f_{cr}}$ is the critical Richardson number, Ke_{cr} is the critical Keulegan number and Λ_0 is a dimensionless constant taken to be 13.3. In this model, the transition from free to forced convection is governed by the critical Richardson number, while the transition from intermediate to high wind speed and surface wave-breaking is defined by the critical Keulegan number. Under clear sky conditions the surface fluxes are to first order determined by the wind speed (Wick et al., 1996). It is therefore possible to gain insight into the characteristics of the skin models by plotting them against wind speed. This is shown in Figure 2.1 and it is evident that the Fairall model exhibits a marked trend with wind speed, whereas Soloviev and Schlüssel's model exhibits a fairly constant range in ΔT.

When using measured data for determining the skin effect, it is useful to consider the complete measurement budget. For the bulk-skin temperature difference measurement it can generally be written as:

$$\Delta T' = T'_{bulk} - T'_{skin} = (T_{bulk} + \delta_b) - (T_{skin} + \delta_s) = \Delta T + \delta_b - \delta_s \qquad (2.4)$$

where ΔT' is the measured bulk-skin temperature difference, δ_b represents errors related to the mixed layer temperature measurement and δ_s represents errors related to the radiometric skin temperature determination. It is evident that δ_b can become large when, as in the presence of a diurnal thermocline, the assumption of a wellmixed layer immediately beneath the skin layer breaks down. Similarly δ_s contains errors associated with the calibration of the skin algorithm based on simulated radiances due to inaccuracies in the radiative transfer modelling. Additionally, in the case of observations from space, errors introduced by contributions from the atmosphere influence δ_s. These points are illustrated by the fact that on simulated radiance datasets biases very close to 0 are obtained, whereas on matchup data larger biases are found. In the following it should be noted that generally the absolute biases are not of concern since they can easily be adjusted, whereas the standard deviation and the impact on it (equivalent to reduction in it) directly quantify the performance of the skin SST algorithms and skin layer parameterisations, respectively.

3. Measurements of SST

For the determination of algorithm performance and skill of the skin models Matchup DataBases (MDB) of satellite passes and in-situ observations have been used. The Pathfinder MDB (Podesta et al., 1997) consists of global quality controlled in-situ buoy observations obtained from the Global Telecommunications System (GTS) as well as from several major research projects and institutions matched to AVHRR GAC (Global Area Coverage, 4 km pixel resolution) data. Centred at each buoy observation a 5x5 pixel box is extracted, SST is calculated based on the Pathfinder algorithm and calibrated as well as raw values are stored. Subsequently a sensor specific cloud clearing scheme is executed and cloud contaminated observations are flagged. In addition to this, a test also used in the SAF retrieval algorithm development (Brisson et al., 1998) is used to remove a few hundred outlying brightness temperature observations that appear cold compared to the in-situ SST. This number is in accordance with a misclassification rate of matchups classified falsely as cloud free of about 2.1% found by the Pathfinder development team (Podesta, personal communication, 1999). An observation is rejected if the following is true:

$$T_{in\text{-}situ} - T_4 > 2.9\,(T_4 - T_5) + 2.3 \qquad (3.1)$$

After this step a symmetric histogram of ΔT is obtained, which is taken as confirmation of a good quality cloud clearing.

The in-situ data in the Pathfinder data set contain information on air temperature and sea surface temperature at some depth, which for the drifters is unspecified, while for the moored buoys it can to some extent be obtained from the suppliers of the original data. In general the drifters do not measure atmospheric properties other than air temperature and pressure. Moored buoys on the other hand often measure several additional parameters, of which only the wind speed is included in the Pathfinder data set. They are typically available from the supplier of the original in-situ data, however. Additionally, auxiliary information is added to each observation in the dataset such as depth of the water column, weekly analysed SST (Reynolds and Smith, 1994) and columnar water vapour content computed from Special Sensor Microwave/Imager (SSM/I) brightness temperatures. See table 3.1 and Figure 3.1 for an overview of data set characteristics. Note that the drifter data generally represent most latitude bands well, however with some overrepresentation of the mid latitudes and that moored buoy observations in the Atlantic are confined to an area along the North American East Coast between 25°N and 43°N.

Buoy types	**Atlantic Drifters**	**Atlantic Moored**	**TOGA-TAO**
# of obs.	7925	2226	2533

Table 3.1 *Overview of the cloud cleared matchups from the Pathfinder dataset used. Moored buoys including the TOGA-TAO dataset generally feature in-situ measurements of wind and in some cases humidity.*

For the problem at hand the information featured in the Pathfinder data set is not sufficient and information on sea surface fluxes and wind speed must be supplied from other sources. For the Atlantic subset of the 1997 NOAA-14 Pathfinder MDB Numerical Weather Prediction (NWP) model representations of net heat flux (latent+sensible+infrared fluxes) leaving the ocean surface as well as wind speed and Wind Mixing Energy (WME) were extracted based on 6-hourly analyses from the UK Met. Office (UKMO) Unified Model and from the European Centre for Medium-Range Weather Forecasts (ECMWF) NWP model. The wind mixing energy is equivalent to wind stress and since the ECMWF model does not output WME, wind stress was extracted in its place. The wind fields are instantaneous, whereas fields of fluxes and wind stress are 6-hour averages. As previously mentioned solar fluxes were omitted since their direct impact on the skin temperature gradient is negligible. For a very limited set of buoys, mainly from the National Data Buoy Center (NDBC) in the Atlantic and for the TOGA-TAO array in the Pacific it was possible to retrieve additional in-situ information on surface humidity from the respective web sites, thus enabling the computation of in-situ fluxes using bulk parameterisations. ECMWF data were extracted for the TOGA-TAO array to further enable a comparison with in-situ data.

4. Assessing the Retrieval Algorithms

From work carried out previously in the frame of the SAF project at CMS and DNMI (Brisson et al., 1998; Eastwood, 1998) there are two potential candidate algorithms for operational SST processing which are the non-linear temperature dependent algorithm and the triple window algorithm.
The non-linear algorithm includes a "first guess" SST from a background field and has the following form:

$$SST = D.\ T_{11} + (A_t.\ T_{guess} + A_s.\ S).(T_{11} - T_{12}) + C \qquad (4.1)$$

where coefficients D and C depend linearly on the secant of the satellite viewing angle.
Two sets of coefficients were derived using representative atmospheric states from databases of radiosoundings globally and for the region of the Atlantic above 50°N latitude (hl), respectively.

The triple window algorithm uses the 3.7 micron channel and so can only be used for night-time scenes. It is of the form:

$$SST = E.\ T_{3.7} + F.\ (T_{11} - T_{12}) + G \qquad (4.2)$$

where coefficients E, F and G were calculated using global data and depend linearly on the secant of the satellite viewing angle.
The hl and global forms of the non-linear algorithm were initially compared by comparing the bulk-skin SST difference or observed ΔT for observations in the Pathfinder MDB above a latitude of 50°N. The Results are shown in Table 4.1

	Observed ΔT (K) (buoy -satellite)					
	Non-linear hl		Non-linear global		Triple window global	
	bias	stdev	bias	stdev	bias	stdev
Night Observations	-0.21	0.55	-0.35	0.57	-0.14	0.45
All Observations	-0.31	0.52	-0.26	0.54	na	na

Table 4.1 *Observed ΔT (buoy-satellite) for Atlantic Pathfinder Matchups above a latitude of 50°N. The matchups include both moored buoys and drifters.*

For both night-time and day-time cases at high latitude the two forms of the non-linear algorithm give very similar results and so, in the context of the skin/bulk study, can be considered equivalent. In subsequent results the global form of the non-linear algorithm is applied. The triple window algorithm gives the best performance in terms of standard deviation which was also found in the low latitude matchups.
It is important to check if there are any trends in the retrieval algorithms with atmospheric parameters such as water vapour loading since these trends could potentially mask the surface skin effect. A histogram of the mean observed bulk-skin SST difference for night-time Atlantic matchups with increasing water vapour loading is shown in Figure 4.1. The non-linear algorithm shows a slight trend of over-estimating the skin SST with increasing water

vapour, whilst the triple window algorithm is very stable. It is also interesting to note that the sign of the bulk-skin SST difference is negative. Since the heat flux between the ocean and atmosphere in clear sky conditions is almost always out of the ocean and atmospheric contamination generally lowers the retrieved skin SST, it would be expected that the skin SST should be cooler than the bulk (i.e. the satellite SST is cooler than the buoy SST). As mentioned earlier, this bias is probably due to the radiative transfer modelling. The observed ΔT trend with satellite zenith angle was also investigated (Figure 4.2). Both algorithms tend to underestimate the skin SST at high zenith angle. To reduce this effect in subsequent results observations are only used with a satellite zenith angle below 60° (secant less than 2.0).

A first look at the effect of surface meteorological conditions was made by forming a histogram of observed ΔT against the NWP 10 m windspeed and this is shown in Figure 4.3 for moored buoys in the Atlantic. The skin SSTs from both retrieval algorithms appear to become warmer with respect to the underlying bulk as the windspeed picks up. This trend follows the concept of the Saunders model; as the windstress on the skin layer increases the depth of the layer is reduced and so the temperature difference between the skin and the bulk is reduced. A similar windspeed trend was observed using ATSR matchup data.

No trend was found with surface windspeed for the Atlantic drifters. This is unexpected since most of the drifters measure at about 20cm depth and so the drifter-satellite SST difference represents more closely the temperature difference across the skin layer than the moored-satellite SST difference. However, it is likely that the drifters are more prone to measurement error than the moored buoys for several reasons, such as their design and prolonged exposure at sea without maintenance. For the drifter measurements to be useful in studying the skin effect more stringent quality control is probably necessary than can be performed in this study.

5. Results of Testing the Skin Layer Models

5.1 Atlantic Moored Buoys

Based on the results from the previous section the models were tested on matchups with moored buoys, which in the 1997 Pathfinder dataset are located along the eastern coast of the USA, from the Gulf of Mexico to Canada. In order to avoid coastal effects in both the in-situ measurements and in the NWP data a subset was selected which contained moored buoys in offshore locations. To further avoid problems with near surface heating during the day only night-time matchups were used and the results are shown in Table 5.1

The success of each model is measured by the reduction in (also termed impact on) the observed ΔT standard deviation. Using the Fairall model on SSTs calculated by the triple window algorithm the standard deviation falls by 0.03K. The value of λ_0 which best fits the observations was 4.5 and is in the range found from experiments at sea. Figure 5.1 shows the results and a positive correlation between the model and the observations can be seen. When the Soloviev-Schlüssel model is applied there is no impact. It is interesting to note that both models predict a similar bias in the bulk-skin SST difference of about 0.25K. The predictions were generated using NWP data from the UK Met. Office atmospheric model with the 6-hourly wind mixing energy providing the estimate of friction velocity. When the NWP 10 m wind was used results deteriorated slightly. Similar results were found when the models were driven by data from the ECMWF atmospheric model, with the Fairall model again making a positive impact.

Case	**Observed ΔT (buoy-satellite) (K)**		**Predicted ΔT (bulk - skin) (K)**		**Observed - Predicted (K)**	**correlation coefficient**
	bias	stdev	bias	stdev	stdev	
Fairall (λ_0 = 4.5) triple window alg.	-0.55	0.29	0.23	0.13	0.26	0.42
Soloviev-Schlussel triple window alg.	-0.55	0.29	0.25	0.12	0.29	0.22
Fairall (λ_0= 4.5) non-linear alg.	-0.74	0.37	0.23	0.13	0.37	0.18
Soloviev-Schlüssel non-linear alg.	-0.74	0.37	0.25	0.12	0.41	-0.13

Table 5.1: *A comparison of the results of applying the skin layer models to the offshore moored buoy night-time matchups. The correlation coefficient represents the correlation between observed ΔT and predicted ΔT. The number of observations in the dataset is 104.*

If the noisier non-linear retrieval algorithm is used to generate the Skin SSTs the skin effect cannot be accounted for by the skin layer models. The Fairall model no longer makes an impact and the Soloviev-Schlüssel model actually adds noise to the data by increasing the standard deviation. Figure 5.2 shows the results using the non-linear algorithm.

The offshore dataset is however quite small and is only made up of observations from 5 buoys. Table 5.2 shows the results of applying the Fairall model to all the matchups at night containing moored buoys. In the case of the triple window algorithm the impact is negligible and the correlation between observations and predictions is much smaller than for the offshore subset. The best fit value of λ_0 is also much lower. If the non linear algorithm is used to retrieve the skin SST then the Fairall model appears to have no skill at all in predicting the observations.

Case	**Observed ΔT (buoy-satellite) (K)**		**Predicted ΔT (bulk - skin) (K)**		**Observed - Predicted (K)**	**correlation coefficient**
	bias	stdev	bias	stdev	stdev	
Fairall (λ_0 = 2.1) triple window alg.	-0.59	0.35	0.12	0.07	0.35	0.17
Fairall (λ_0= 2.1) non-linear alg.	-0.66	0.46	0.12	0.07	0.46	-0.01

Table 5.2: *A comparison of the results of applying the skin layer models to all Atlantic moored buoy night-time matchups. The number of observations in the dataset is 615.*

From these two studies it appears that in moving from an offshore dataset to a larger dataset with a wider range of atmospheric and ocean conditions other effects dominate and the skin effect becomes negligible.

5.2 The TOGA-TAO Array

Another set of moored buoys which can be used to investigate the skin effect is the TOGA-TAO array in the tropical Pacific. The array is routinely maintained so the SSTs should be of a high quality. Another advantage of using the array is that the atmospheric observations made by each buoy can easily be obtained from the TOGA-TAO website. The NWP analyses will tend to smooth out local atmospheric features such as gusts and surface humidity which may impact on the skin layer predictions. In order to see whether the skin layer models are more effective if they are driven by in-situ data rather than with data from NWP models, atmospheric data corresponding to pathfinder matchups was obtained for 7 TOGA buoys in the eastern Pacific. Surface fluxes were generated using the bulk parameterisation scheme due to Fairall et al. (1996b). The results are shown below in Table 5.3 for predictions driven by both NWP data and in-situ measurements. Using the NWP data a small positive impact is observed with the Fairall model, however there appears to be no benefit in using in-situ fluxes on the dataset. It is worth mentioning that the variability in terms of standard deviation in fluxes and wind speed of the TAO dataset is respectively 25% and 50% lower than that observed for the Atlantic offshore dataset. This fact is clearly reflected in the low standard deviation of the resulting predicted ΔT and may in part explain the low impact. Note also that the mean bulk-skin predictions are independent of the type of meteorological data used to drive the models.

Case	Observed ΔT (buoy-satellite) (K)		Predicted ΔT (bulk - skin) (K)		Observed - Predicted (K)	correlation coefficient
triple window alg.	bias	stdev	bias	stdev	stdev	
NWP flux and wind:						
Fairall (λ_0 = 4.0)	-0.19	0.24	0.17	0.06	0.23	0.26
Soloviev-Schlüssel			0.23	0.05	0.24	0.24
in-situ flux and wind:						
Fairall (λ_0= 4.0)	-0.19	0.24	0.17	0.05	0.24	0.20
Soloviev-Schlüssel			0.23	0.04	0.24	0.16

Table 5.3: *A comparison of the results of applying the skin layer models to TOGA-TAO moored buoy night-time matchups. The number of observations in the dataset is 196.*

5.3 The Geographical Distribution of the Skin Effect in the Atlantic

It is instructive to look at the variation of the Fairall model predictions across the Atlantic and this is shown in Figure 5.3 for each moored and drifting night-time matchup location. The mean bulk-skin difference is 0.21K with peak predictions rising to 0.8K at a latitude of about 35°N. At high latitudes where in general surface windspeeds tend to be higher the predictions are much smaller and so the skin effect can effectively be neglected in this case. Figure 5.4 shows observed ΔT at night for the Atlantic. The observations appear to have the largest range in the same latitude band as the predictions. Figure 5.5 reveals that the peak predictions seem to coincide with the Gulf Stream, moving across the Atlantic to the European coast. This is exactly where large surface heat fluxes are expected to be present in the winter months. Otherwise, peak predictions are observed in the Mediterranean and in the Indian Ocean. It also shows that the predictions at the equator are generally low as experienced with the TAO dataset. When comparing to Figure 5.6 a good general agreement of the patterns of the bulk-skin temperature difference with peaks coinciding is noted although as is already seen in Figures 5.3 and 5.4 the predicted range is much smaller than the observed.

6. Conclusions

In the present report it has been shown that at best the skin models account for a positive impact of between 0.01 to 0.03 in the standard deviation of the buoy-satellite SST difference. In keeping with this small impact it has been shown that once the level of noise in the skin retrieval is raised the skin effect is masked out. Thus, the best results were found with the triple window skin SST algorithm, that has been shown to be very stable with respect to atmospheric effects. In terms of modelling the skin effect, the largest impact was found using the Fairall model, while the Soloviev-Schlüssel model displayed near zero impact in most cases. It should be stressed that the impacts observed were very low, however the distribution of ΔT with wind speed is found to follow the characteristics of the Fairall model closer than the characteristics of the Soloviev-Schlüssel model (see Figures 2.1 and 6.1), especially at low windspeed. This is an important result because previous studies have tended to lack observations at low windspeed (e.g. Wick et al,1996). Using meteorological data from different sources (both NWP and in-situ) did not significantly change the results. When using NWP data the best impact was found using the 6-hour averaged friction velocity (from either the windstress or wind mixing energy) rather than the instantaneous 10 m windspeed. This is probably because in converting from the 10 m wind to the surface friction velocity an assumption was made of neutral stability, whereas the NWP models include detailed boundary layer modelling.

An interesting observation from Figure 6.1 is that the TOGA-TAO observed ΔTs are consistently larger than those from moored buoys in the Atlantic. This probably indicates residual cloud contamination in the tropical Pacific and may, together with the observed lower variability in fluxes and wind, explain the smaller impact of the skin models in this region.
The skin layer models were only tested on night-time matchups since during the day under low windspeed and high insolation conditions the assumption of a well mixed layer below the skin breaks down, due to the build-up of a near surface thermocline. There was abundant evidence in the day-time matchups of thermocline events in both the Gulf of Mexico and in the Mediterranean, locations where clear skies and calm conditions prevail in the summer months. A method which could mask out this effect is to study matchups in the moderate to high windspeed regime.

Across the Atlantic the two skin layer models predicted a mean bulk-skin SST difference of about +0.2K, whilst the observations were negatively biased and exhibited a larger range. There are marked geographical differences in both the predictions and the observations. The skin effect peaks in the mid latitudes, while displaying minimal values in the high latitudes.
For the operational production of SSTs by the SAF the benefits of using skin layer models to convert to a bulk product seem minimal when the computing overhead of accessing NWP data is considered. In particular, if the non-linear SST algorithm is adopted as the operational skin retrieval method, errors far larger than the bulk-skin difference will exist in the data and mask its effect completely.

7. Acknowledgements

This work was carried out at CMS Lannion as a visiting scientist project for the Ocean and Sea-ice SAF. Thanks go to Pierre Le Borgne and Steinar Eastwood (DNMI) for fruitful discussions on the skin SST retrieval methods for AVHRR. Anne Marsouin provided useful software for manipulation of the matchup data. Hervé Roquet helped the authors obtain ECMWF NWP data and also contributed to various discussions on the skin effect. Finally the authors thank the staff at CMS Lannion for their hospitality during the visit.

8. References

Andersen S, A. Brisson, S. Eastwood, P. Le Borgne & A. Marsouin: Developments on SST Retrieval over the Atlantic using Geostationary and Polar Orbiter Satellite Data in the Frame of the EUMETSAT Oean and Sea-Ice Satellite Application Facility, In proceedings of the 9th Conference on Satellite Meteorology and Oceanography, Paris France, 1998.

Brisson A, T Jeandrieu, P Le Borgne, A Marsouin: CMS Matchup Databases, CMS Internal Report, Météo-France, 1997.

Brisson A, P Le Borgne, A Marsouin: Development of algorithms for SST retrieval at O&SI SAF Low and Mid Latitudes, CMS Internal Report, Météo-France, 1998.

Candy B & A R Harris: Skin to Bulk Conversion of Sea Surface Temperatures from ATSR-2, Forecasting Research Technical Report No. 238, United Kingdom Meteorological Office, 1998.

Eastwood S: Report about Visiting Scientist Stay at CMS, Meteo-France, DNMI, Oslo, 1998.

Fairall C W, E F Bradley & G S Young: Cool-skin and warm-layer effects on Sea Surface Temperature, *J. Geophys. Res.,* **101**, 1295-1308, 1996a.

Fairall C W, E F Bradley, D P Rogers, J B Edson & G S Young: Bulk parameterization of air-sea fluxes for the Tropical Ocean-Global Atmosphere Coupled Ocean-Atmosphere Response Experiment, *J. Geophys. Res.,* **101**, 3744-3764, 1996b.

Grassl H: The Dependence of the Measured Cool Skin of the Ocean on Wind Stress and Total Heat Flux, *Boundary Layer Meteorol.,* **10**, 465-474, 1976.

Kent E, T Forrester & P K Taylor: A Comparison of Oceanic Skin Effect Parameterizations using Shipborne Radiometer Data, *J. Geophys. Res.*, **101**, 16649-16666, 1996.

Podesta G P, S Shenoi, J W Brown, R H Evans: AVHRR Pathfinder Ocean Matchup database 1985-1995 version 19.0', http://www.rsmas.miami.edu/~gui/matchups.html, 1997.

Reynolds R W, T M Smith: Improved Global Sea Surface Temperature Analyses using Optimum Interpolation, *J. Climate*, **7**, 929-948, 1994.

Saunders P M: The Temperature at the Ocean-air Interface, *J. Atmos. Sci.*, **24**, 269-273, 1967.

Soloviev A V, P Schlüssel: Parameterisation of the Cool Skin of the Ocean and of Air-Ocean Gas Transfer on the Basis of Modelling Surface Renewal, *J. Phys. Oceanogr.*, **24**, 1339-1346, 1994.

Wick G A, W J Emery, L H Kantha, P Schlüssel: The Behavior of the Bulk - Skin Sea Surface Temperature Difference under Varying Wind Speed and Heat Flux, *J. Phys. Oceanogr.*, 26, 1969-1988, 1996.

9. Figures

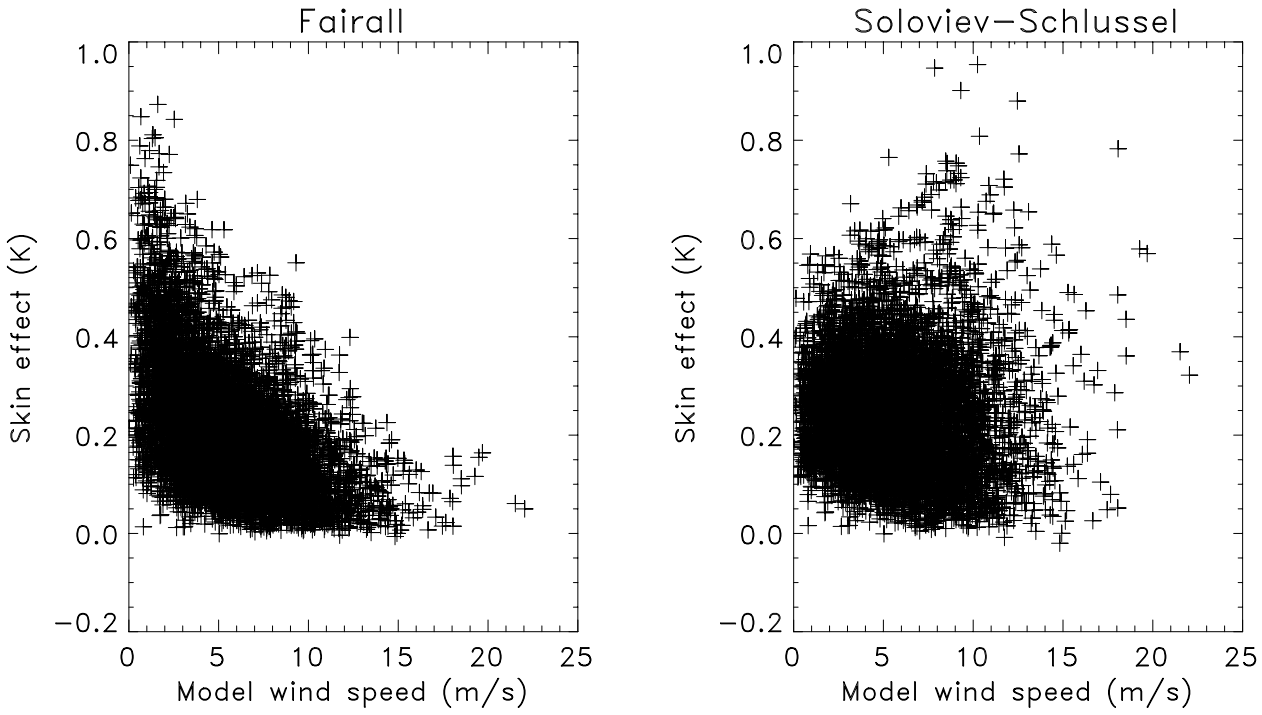

Figure 2.1 *Predictions of the skin effect by the Fairall model (left panel) and the Soloviev-Schlüssel model (right panel). The calculations are based on estimates of flux and wind mixing energy from the UKMO forecasting model for cloudfree locations (matchups) in the Atlantic during 1997.*

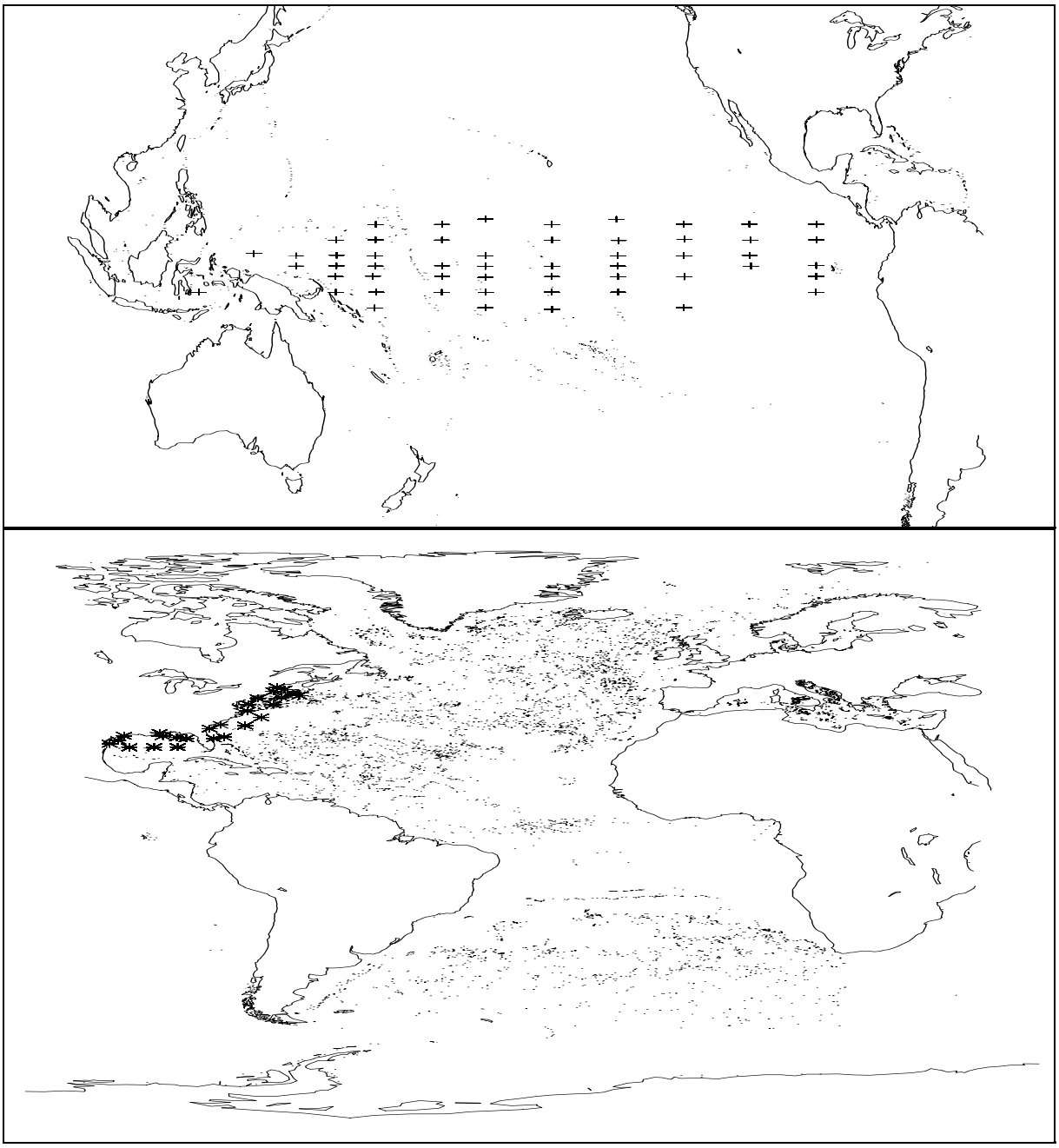

Figure 3.1 *Upper panel shows the locations of TOGA-TAO buoys (+), while the lower panel shows locations of drifters (dots) and moored buoys (*) in the Atlantic ocean present in the Pathfinder matchup database.*

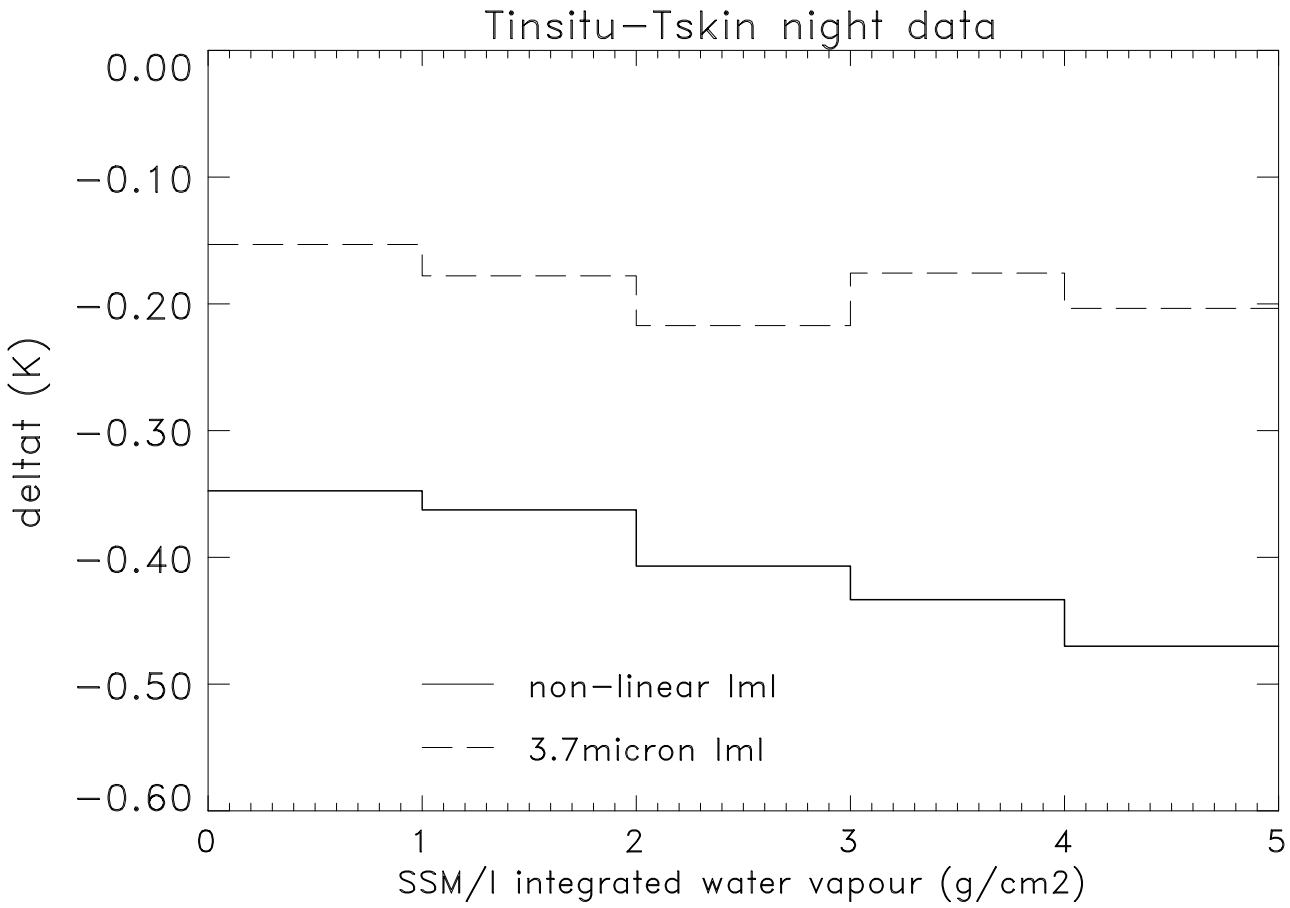

Figure 4.1 *A histogram of the atlantic, nightly observed ΔT (buoy-satellite) against observed water vapour from SSM/I.*

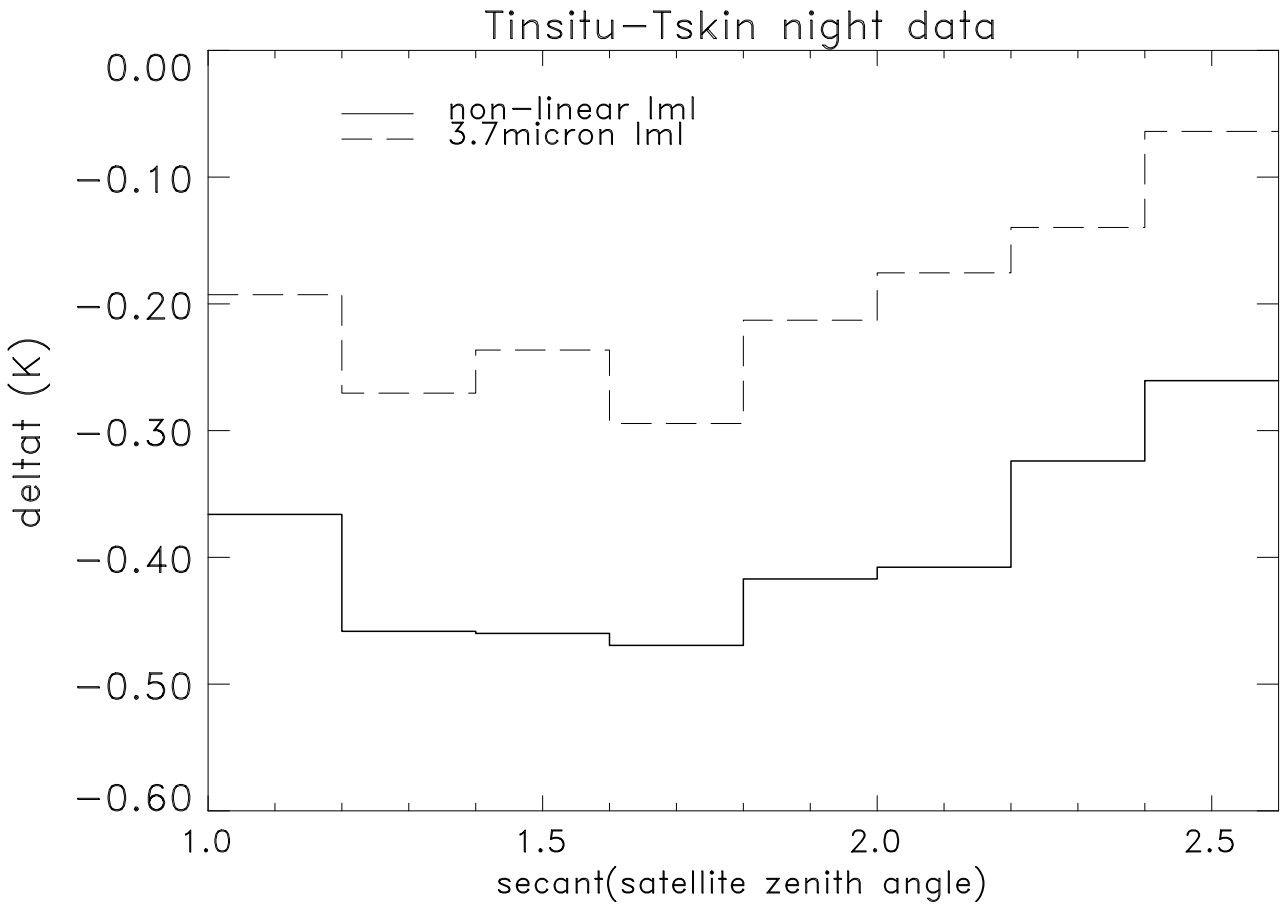

Figure 4.2 *A histogram of the atlantic, nightly observed ΔT (buoy-satellite) against secant of the satellite zenith angle.*

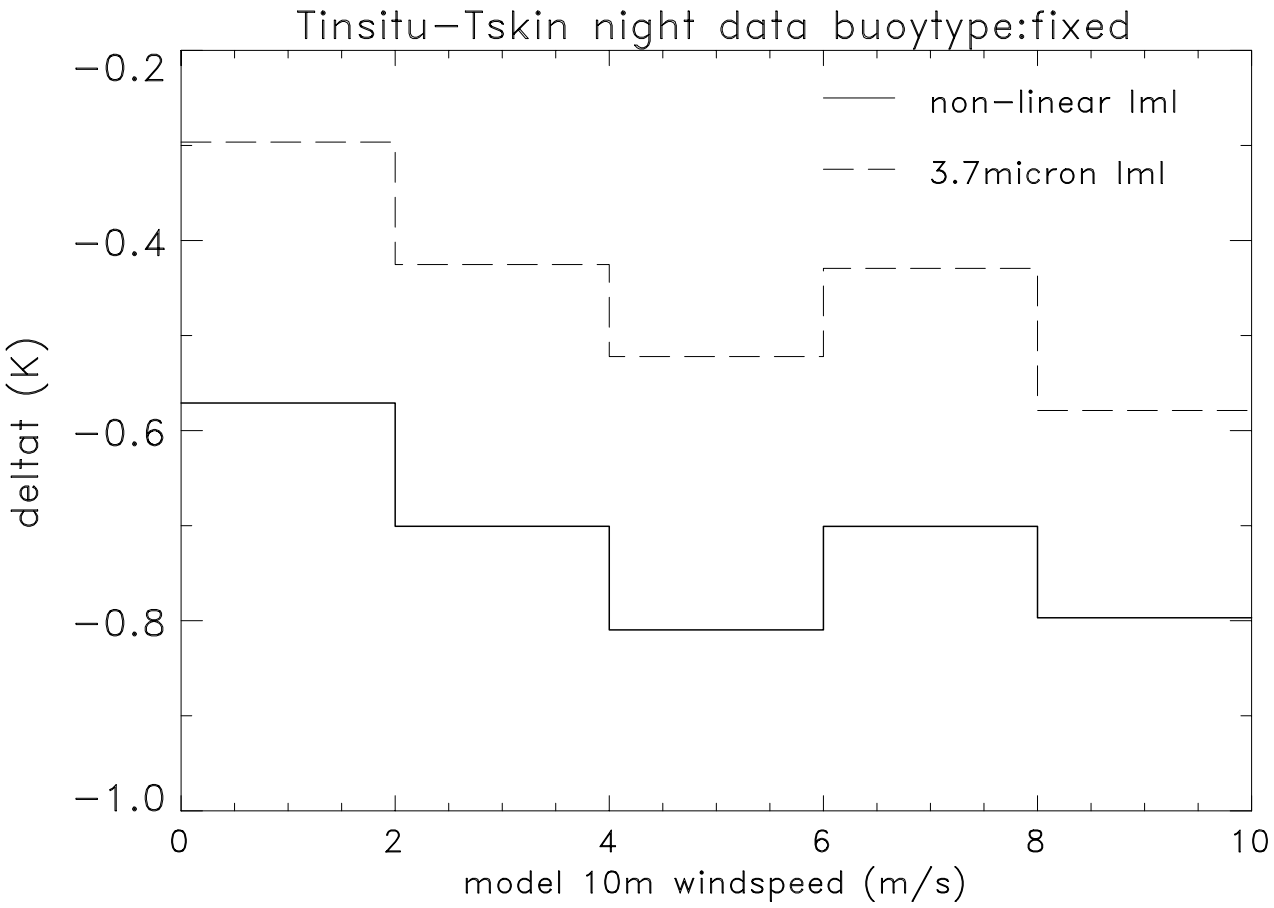

Figure 4.3 *A histogram of nightly observed ΔT (buoy-satellite) from moored buoys in the Atlantic against model 10 m wind speed.*

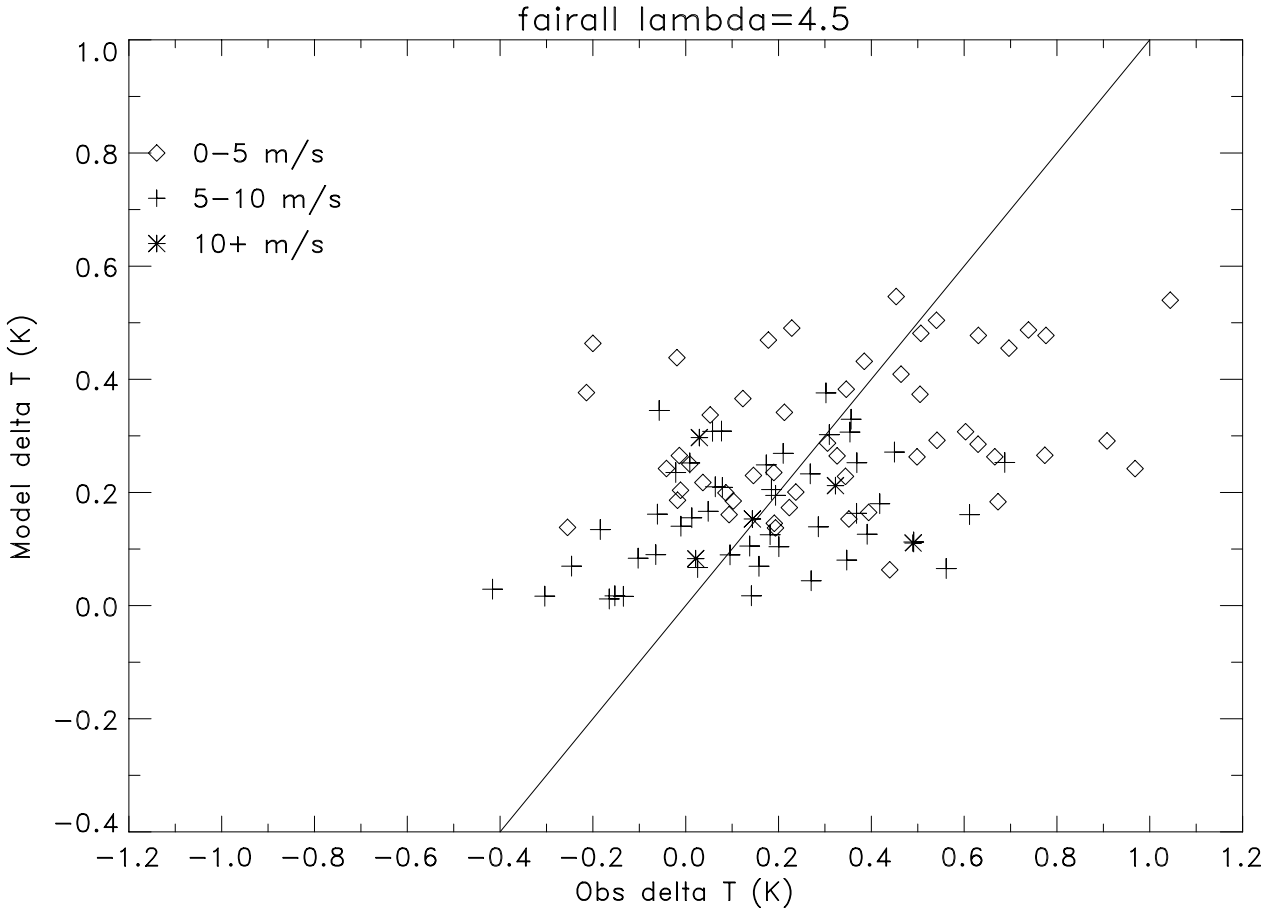

Figure 5.1 *Observed vs. predicted skin temperature difference at different wind speeds for a selection of offshore moored buoys in the Atlantic. The predictions are made using the Fairall algorithm (λ_0 = 4.5) driven by UKMO model wind mixing energy and fluxes. Observed ΔT's are calculated based on the triple window skin retrieval algorithm and bias corrected. Wind speed ranges are indicated as 0-5 m/s (diamond), 5-10 m/s (+) and above 10 m/s (*).*

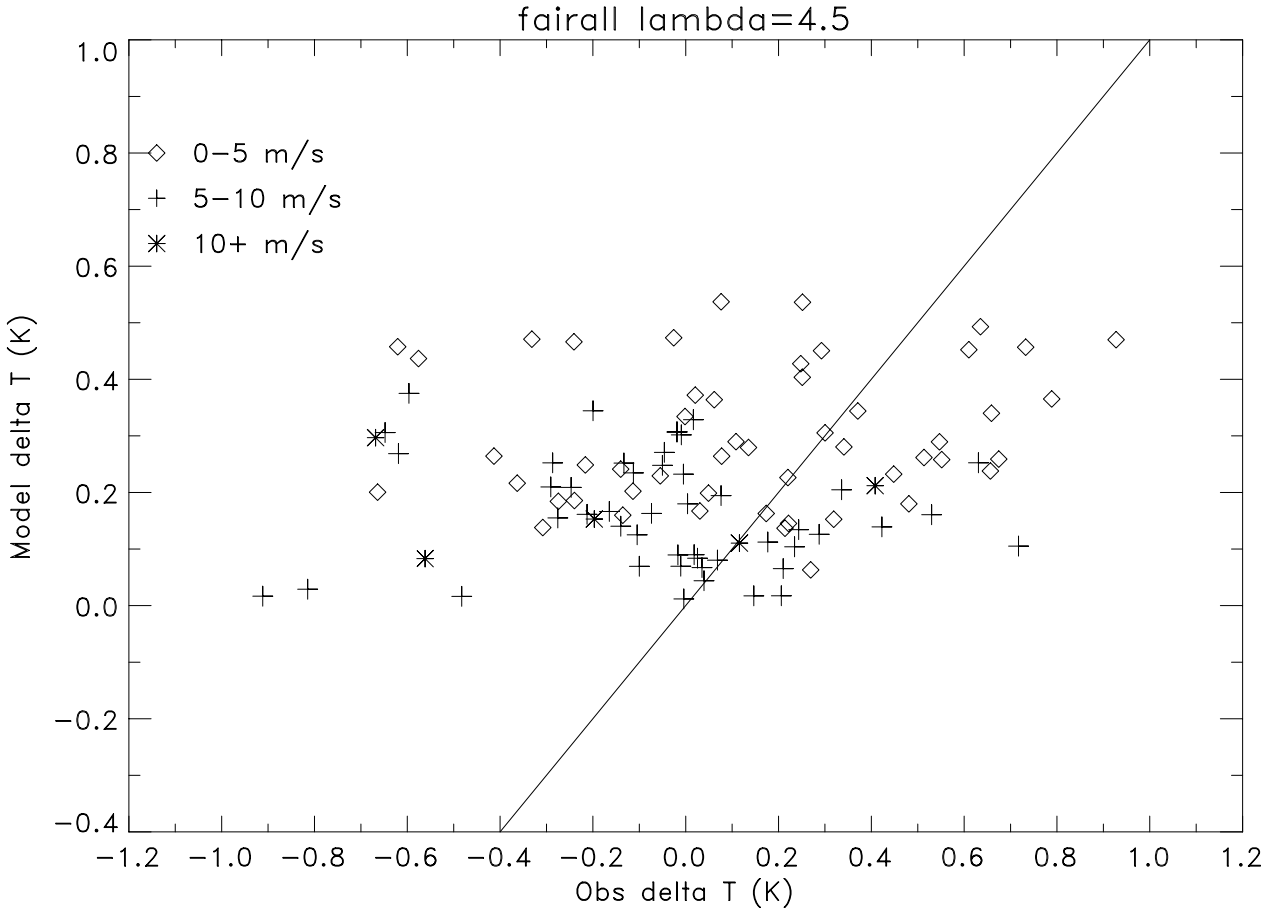

Figure 5.2 *Observed vs. predicted skin temperature difference at different wind speeds for a selection of offshore moored buoys in the Atlantic. The predictions are made using the Fairall algorithm (λ_0 = 4.5) driven by UKMO model wind mixing energy and fluxes. Observed ΔT's are calculated based on the non-linear skin retrieval algorithm and bias corrected. Wind speed ranges are indicated as 0-5 m/s (diamond), 5-10 m/s (+) and above 10 m/s (*).*

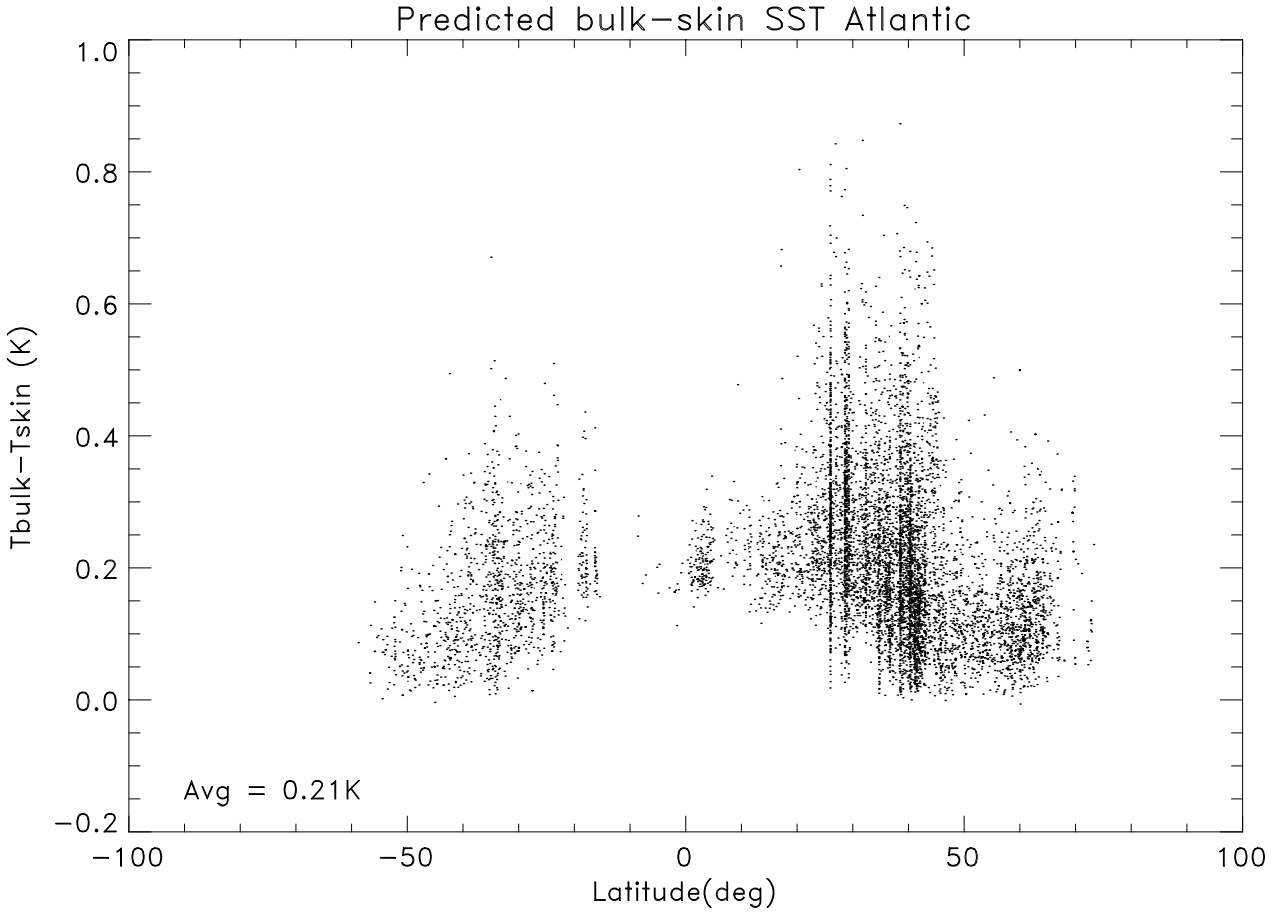

Figure 5.3 *Latitudinal distribution of the predicted bulk-skin temperature difference in the Atlantic computed using the Fairall algorithm with $\lambda_0 = 4$ and based on UKMO model wind mixing energy and fluxes.*

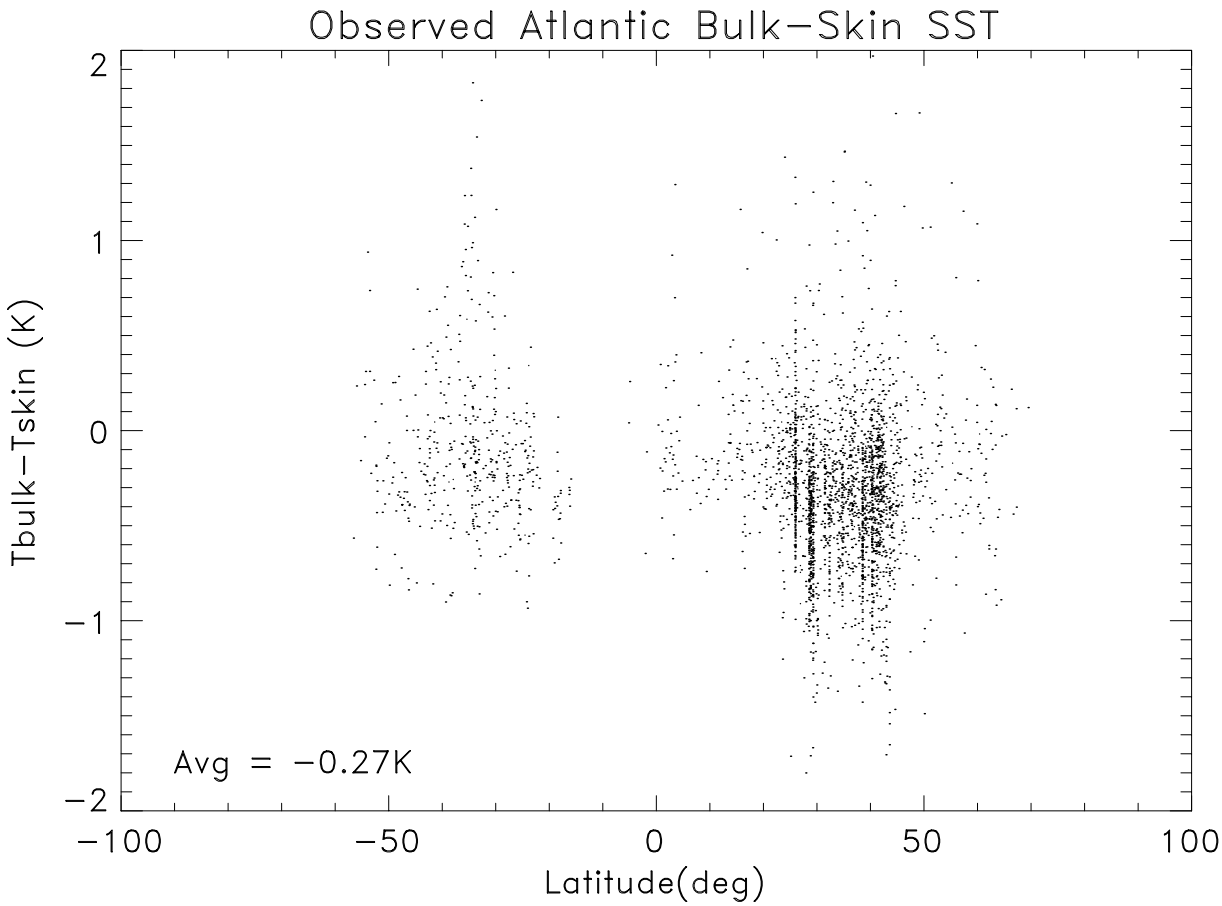

Figure 5.4 *Same as Figure 5.3 but observed based on the nightly triple window algorithm and including both moored and drifting buoys.*

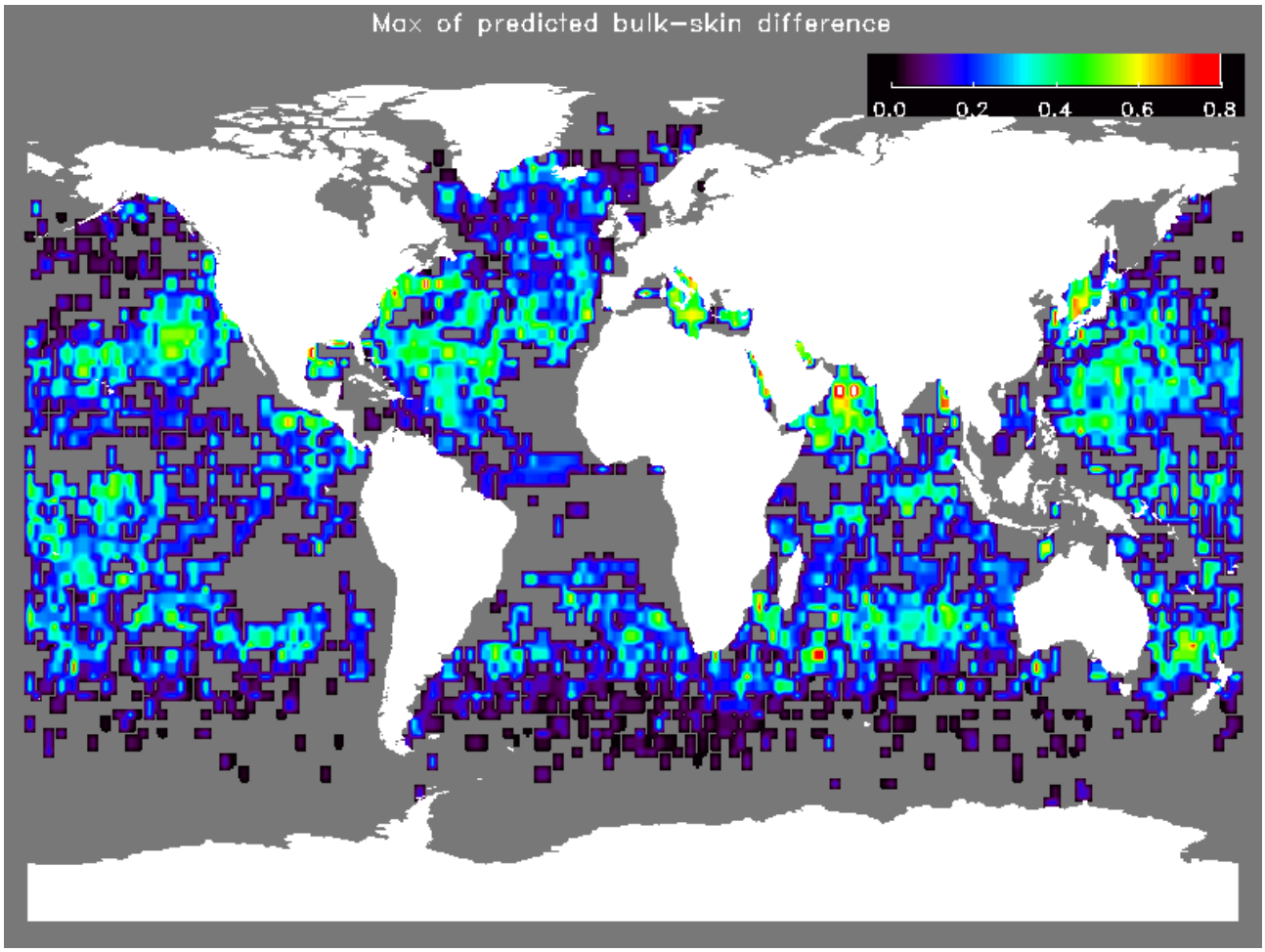

Figure 5.5 *Maximum values of predicted bulk skin temperature differences based on the Fairall skin model taken on a 2x2° grid. Areas of no observations are coloured grey.*

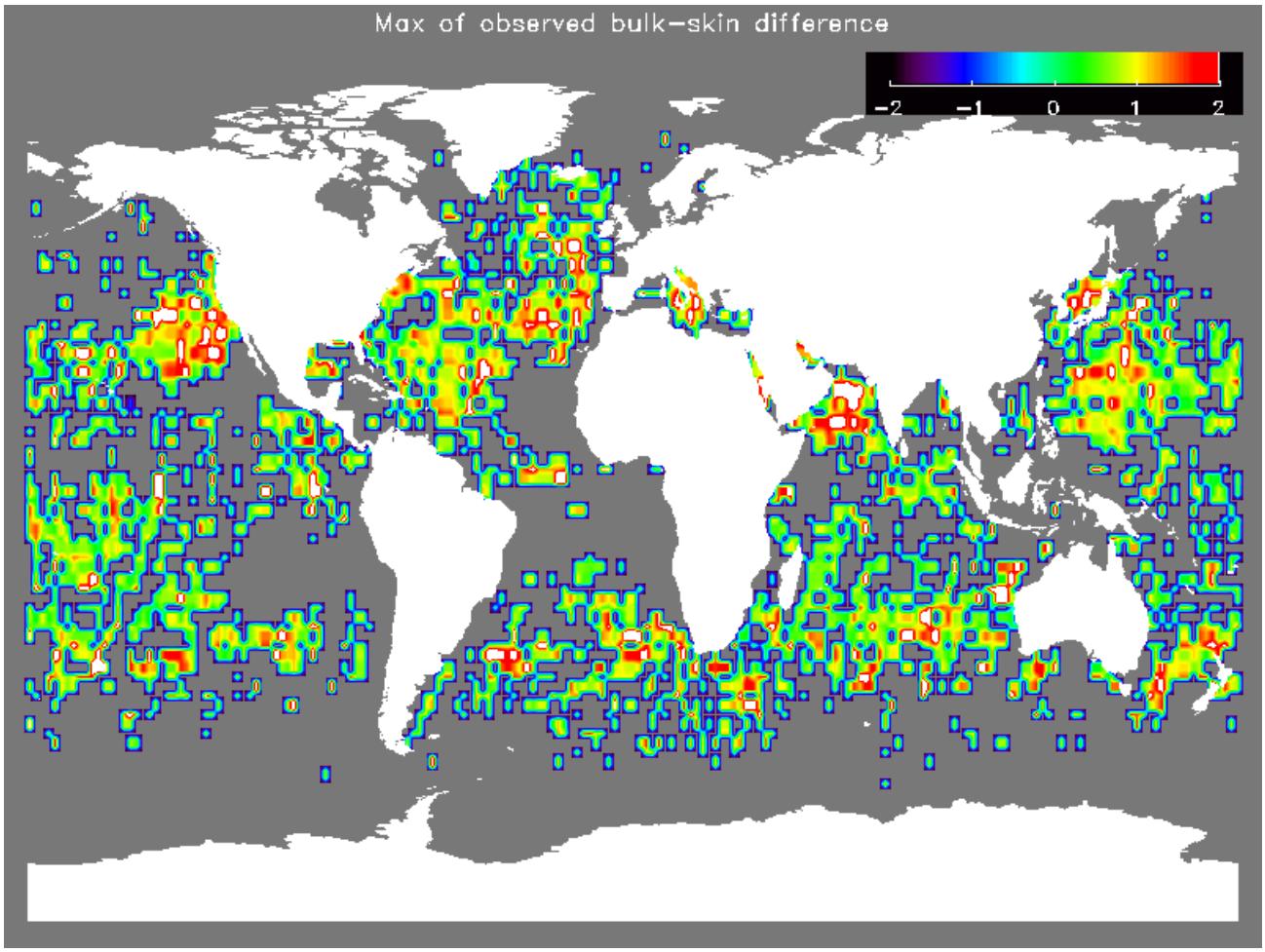

***Figure* 5.6** *Same as Figure 5.5 but observed based on the nightly triple window algorithm and including both moored and drifting buoys.*

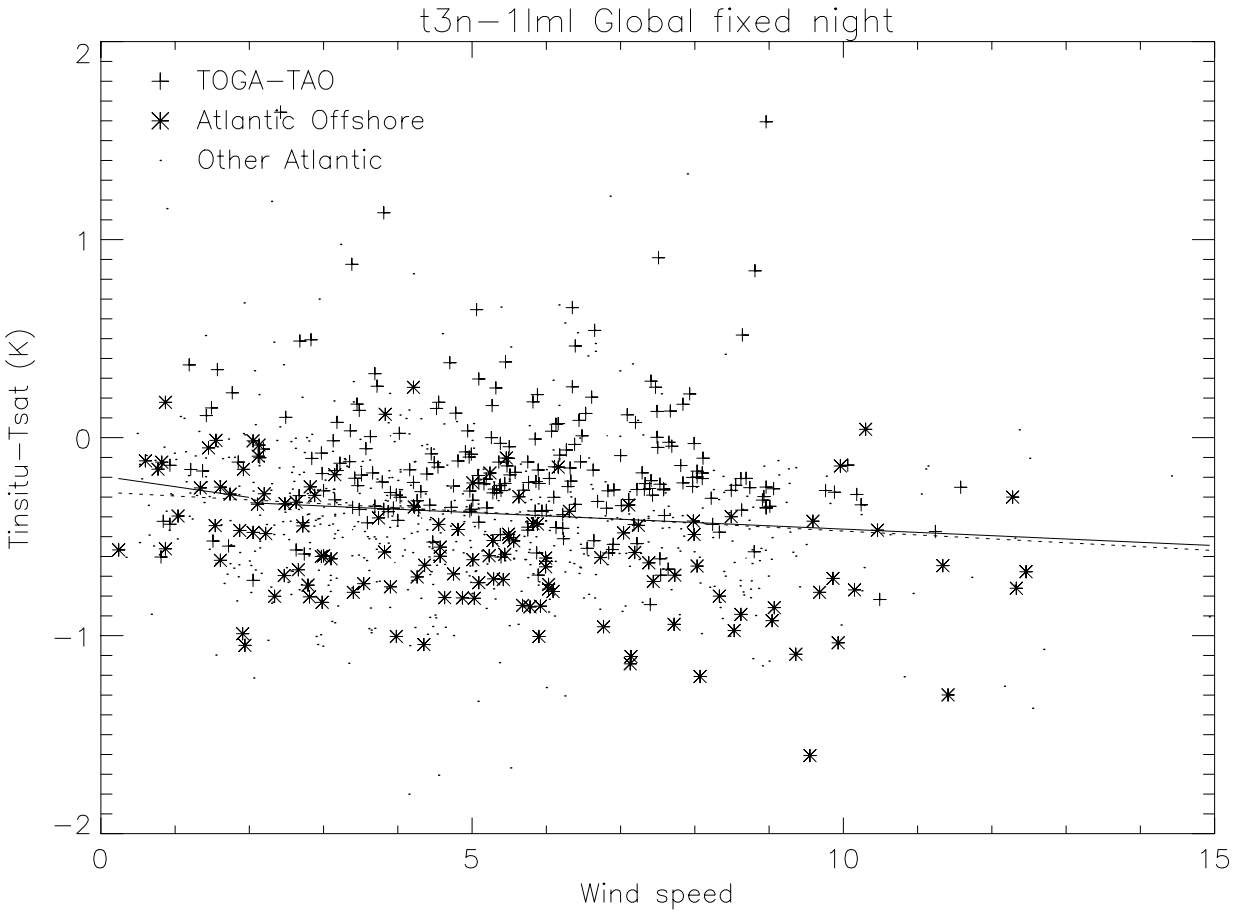

Figure 6.1 *Observed Skin temperature difference based on the triple window retrieval algorithm and observations from the TOGA-TAO array (+), Atlantic offshore moored buoys (*) and other Atlantic moored buoys (dots). The dotted line indicates the best linear fit through all the observations, while the solid lines indicate local fits in the intervals 0-2 m/s and above 2 m/s.*